Electronic Supplementary Information

A Valuable Strategy to Improve Ferroelectric Performance Significantly via Metallic Ions Doping in the Lattice Nodes of Metal-Organic Frameworks

Jingjing Liang, Meiying Liu, Xuebin Xu, and Zhiliang Liu*

Inner Mongolia Key Laboratory of Chemistry and Physics of Rare Earth Materials, School of Chemistry and Chemical Engineering, Inner Mongolia University, Hohhot, 010021, P. R. China

Section S1. Materials and characterization

All chemicals were purchased from commercial sources and used without further purification. Inductively coupled plasma optical emission spectrometry (ICP-OES) measurements were conducted on a PerkinElmer OPTIMA-8000. The transmission electron microscopy (TEM) images and energy dispersive X-ray spectroscopy (EDS) elemental mappings were acquired on a Talos F200X transmission electron microscope at an accelerating voltage of 200 kV equipped with an energy dispersive detector of Oxford INCAEnergy+. The powder X-ray diffraction patterns (PXRD) of the samples were recorded using an Empyrean Panalytical apparatus (Cu Kα, λ = 1.5418 Å). X-ray photoelectron spectroscopy was collected by using ESCALABXI+ from Thermo Fisher Scientific. Differential scanning calorimetry (DSC) was carried out in a nitrogen stream using a TA Q2000 equipment with heating rate of 10 °C/min. Thermogravimetric analysis (TGA) curves were obtained using a Netzsch STA409pc apparatus under a nitrogen atmosphere with a heating rate of 10 °C/min from 30 to 800 °C. The polarization versus electric field (P−E) hysteresis loops were measured on a Radiant Precision Premier II ferroelectric tester at room temperature. The pellets of the powder samples with electrodes made of Ag-conducting glue on the parallel face were prepared to measure the hysteresis loops.

Section S2. Synthesis of Ni-MOF and Mg/Ni-MOFs

2.1. Synthesis of Ni-MOF. $Ni(NO_3)_2 \cdot 6H_2O$ (204 mg, 0.7 mmol) was added to an aqueous solution (10 mL) of isonicotinic acid (25 mg, 0.2 mmol), isophthalic acid (66 mg, 0.4 mmol) and NaOH (44 mg, 1.1 mmol). The mixture was sealed in a 23 mL Teflon-lined autoclave with stainless steel vessel and heated to 185 °C within 8 hours, maintained at this temperature for 60 hours, and then cooled to 30 °C within 48 hours. Blue green block crystals of Ni-MOF were obtained by filtration. The obtained samples were heated to 100 ℃ for 6 hours to remove the remaining H_2O in channels.

2.2. Synthesis of Doped-MOFs. An ethanolic solution (6 mL) of $Ni(NO_3)_2 \cdot 6H_2O$ (184 mg, 0.63mmol) and $Mg(NO_3)_2 \cdot 6H_2O$ (18mg, 0.07mmol) was stirred equably then

added to an aqueous solution (4 mL) of isonicotinic acid (25 mg, 0.2 mmol), isophthalic acid (66 mg, 0.4 mmol) and NaOH (44 mg, 1.1 mmol). The mixture was sealed in a 23 mL Teflon-lined autoclave with stainless steel vessel and heated to 200 °C within 2 hours, maintained at this temperature for 24 hours, and then cooled to room temperature naturally. Light green crystalline powder of doped-MOF-1 was obtained by filtration. And the obtained samples were heated to 100 ℃ for 6 hours to remove the remaining solvent molecules in channels.

Doped-MOF-2, doped-MOF-3, doped-MOF-4 were obtained through replace the stoichiometric value of $Ni(NO_3)_2 \cdot 6H_2O$ and $Mg(NO_3)_2 \cdot 6H_2O$ to 0.595 mmol/ 0.105 mmol; 0.56 mmol/ 0.14 mmol; 0.525 mmol/ 0.175 mmol, respectively, with other conditions unchanged.

Table S1. The ratios of metal ions and formulas of each Mg-doped MOFs.

Compound	**Formula**	**Ni : Mg Feed ratio**	**Ni : Mg Ratio in product**
Doped-MOF-1	$[Ni_{6.74}Mg_{0.26}(OH)_4(H_2O)_2(INA)_4(IPA)_3]$	9 : 1	25 : 1
Doped-MOF-2	$[Ni_{6.66}Mg_{0.34}(OH)_4(H_2O)_2(INA)_4(IPA)_3]$	6 : 1	20 : 1
Doped-MOF-3	$[Ni_{6.59}Mg_{0.41}(OH)_4(H_2O)_2(INA)_4(IPA)_3]$	4 : 1	16 : 1
Doped-MOF-4	$[Ni_{6.52}Mg_{0.48}(OH)_4(H_2O)_2(INA)_4(IPA)_3]$	3 : 1	13 : 1

Table S2. The comparison of ferroelectricity between Ni-MOF, doped-MOF-4 and other ferroelectric MOFs.

Name	P_s (μC/cm^2)	P_r (μC/cm^2)	E_c (kV/cm)	Ref.
Ni-MOF	0.1	0.004	2.5	This work
Doped-MOF-4	0.6	0.2	12.6	This work
$[Sr(DMF)\text{-}(\mu\text{-}BDC)]_\infty$	0.83	0.48	0.81	1
$[Zn(s\text{-}nip)_2]_n$	0.294	0.035	4.08	2
$[[Co(s\text{-}nip)_2]\cdot(H_2O)_{0.5}]_n$	0.033	0.013	3.68	2
$[Zn(Mitz)Cl]_n$	0.51	0.21	2.6	3
$[(EMI)_2[Zn_3(1,2,4,5\text{-}BTC)_2]2H_2O]_n$	0.049	0.018	0.21	4
$[[Dy_2(L)_3(H_2O)_2(DMF)_2]\cdot(DMF)_3\cdot H_2O)]_n$	0.38	0.2	2.09	5
$[Cd(trtr)_2]_n$	0.01	0.004	2.28	6
$[[Cu_2(L)(H_2O)_2]\cdot(4DMF)(4H_2O)]_n$	8	3.5	12	7
$[Cd_2(L)_4(\mu_2\text{-}Br)(Br)(H_2O)]_n$	0.39	0.14	2.37	8
$[Cd_2(L)_4(\mu_2\text{-}Cl)(Cl)(H_2O)]_n$	0.54	0.17	2.08	8

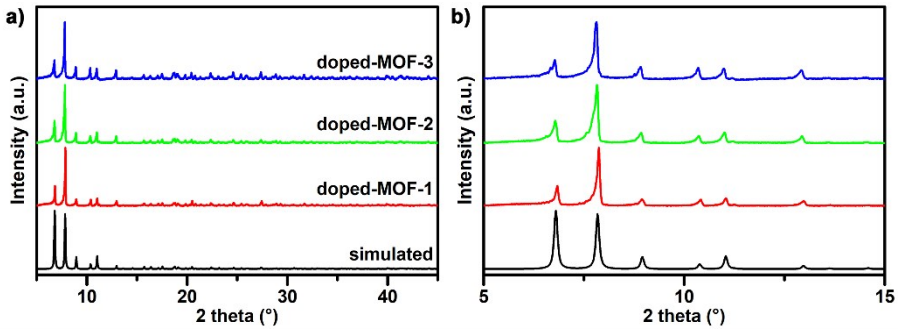

Fig. S1. (a) PXRD patterns of simulated Ni-MOF, doped-MOF-1, doped-MOF-2, and doped-MOF-3. (b) Enlarged PXRD patterns show the detailed comparison of peak positions after Mg^{2+}-doping.

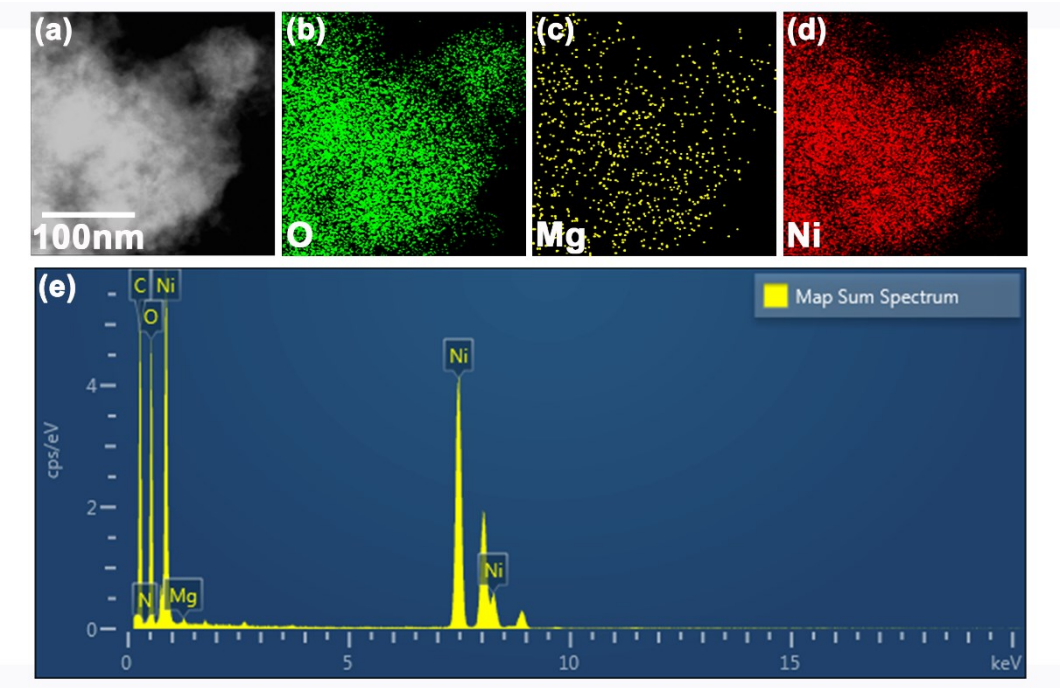

Fig. S2. TEM image (a), EDS elemental mappings (b-d) and spectrum analysis (e) of doped-MOF-1.

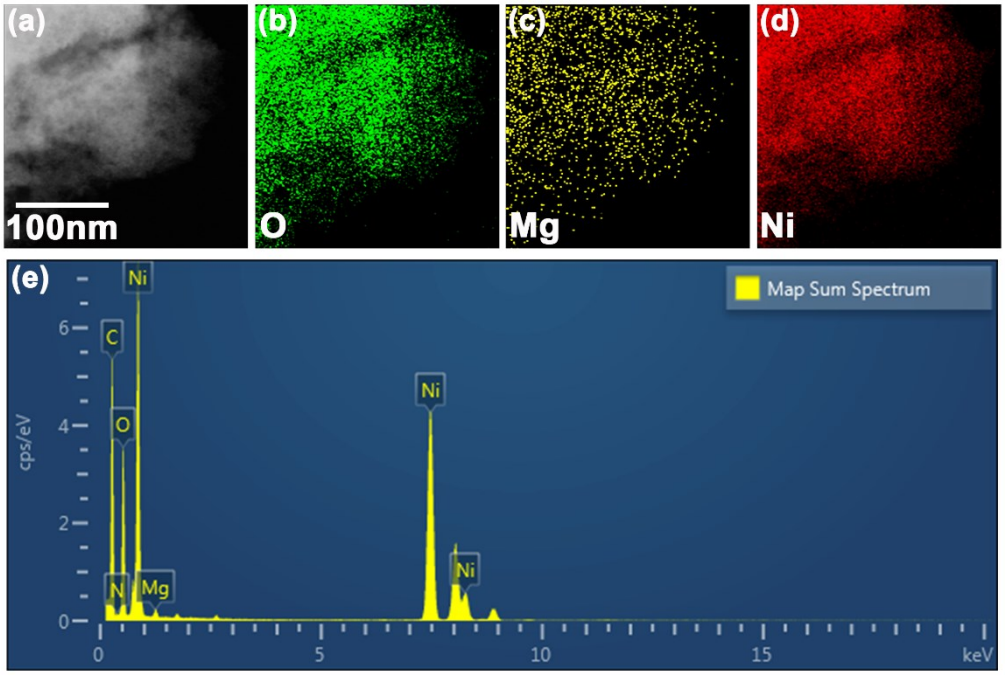

Fig. S3. TEM image (a), EDS elemental mappings (b-d) and spectrum analysis (e) of doped-MOF-2.

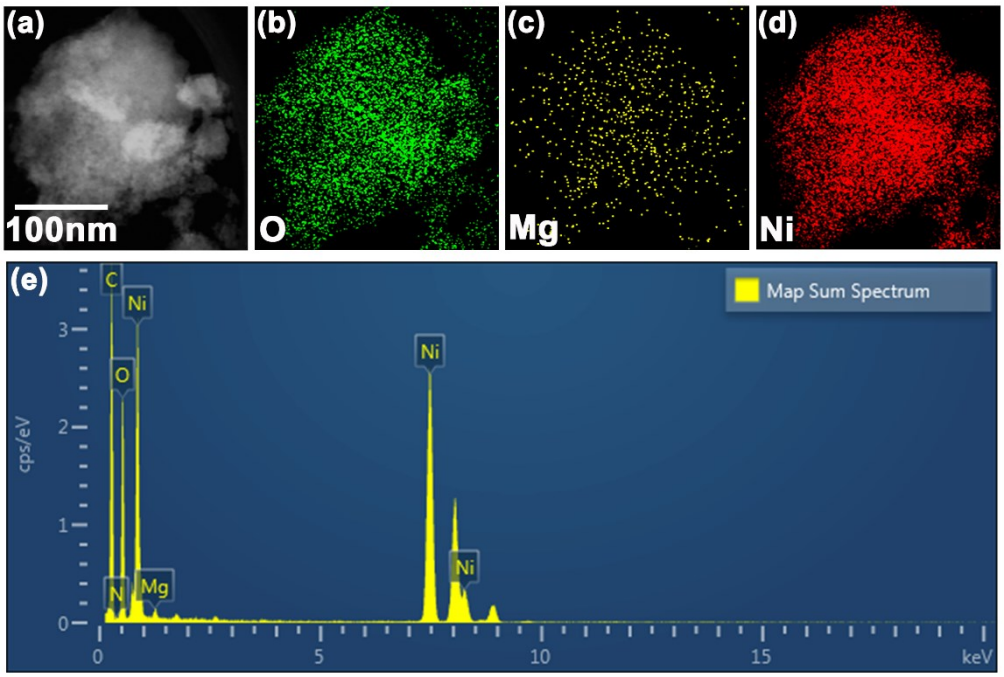

Fig. S4. TEM image (a), EDS elemental mappings (b-d) and spectrum analysis (e) of doped-MOF-3.

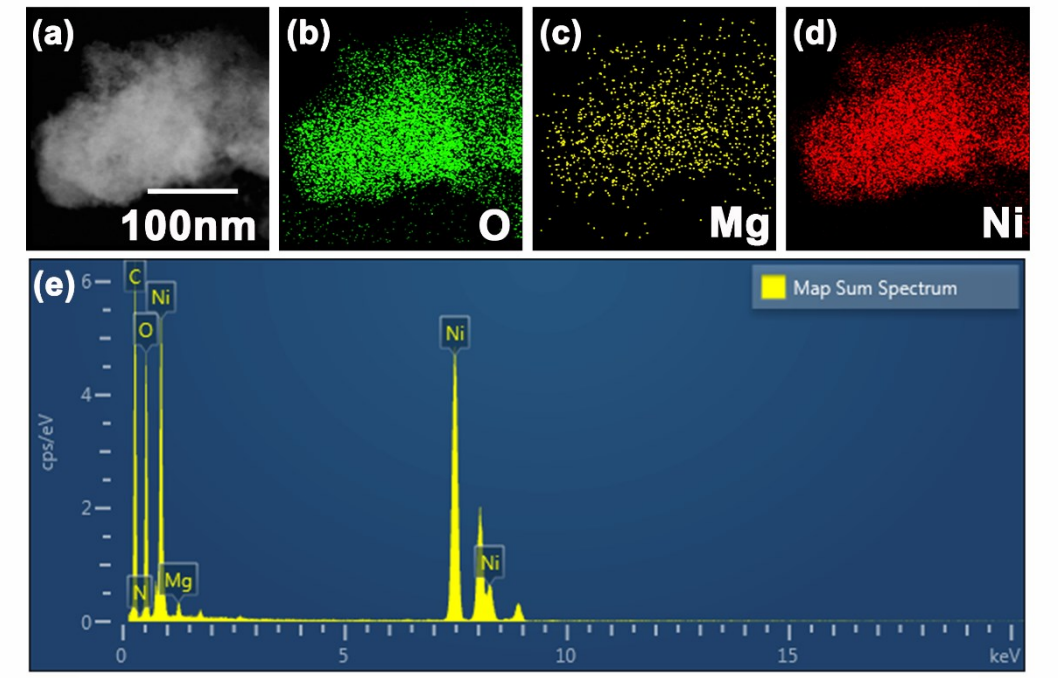

Fig. S5. TEM image (a), EDS elemental mappings (b-d) and spectrum analysis (e) of doped-MOF-4.

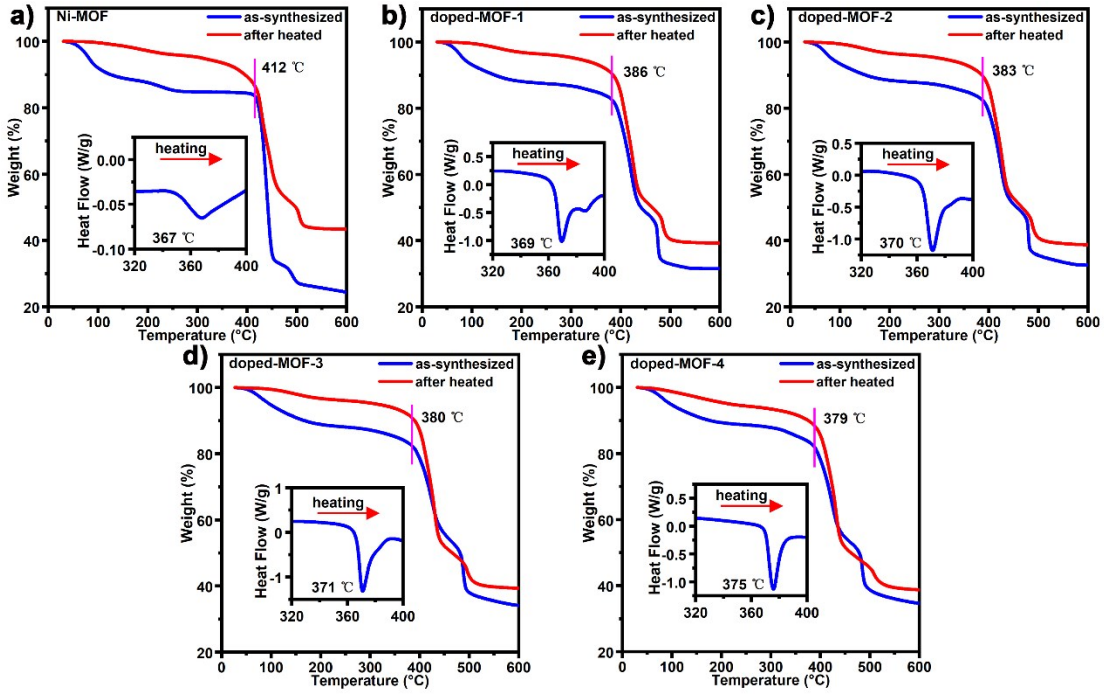

Fig. S6. TGA and DSC (inset) curves of Ni-MOF (a), doped-MOF-1 (b), doped-MOF-2 (c), doped-MOF-3 (d), and doped-MOF-4 (e).

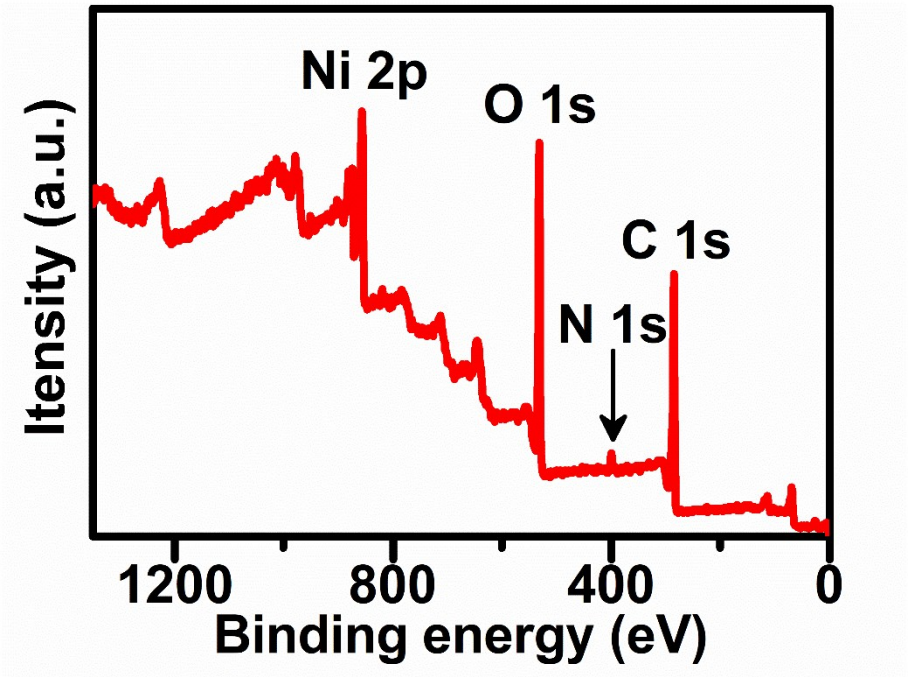

Fig. S7. Survey XPS spectra of undoped Ni-MOF.

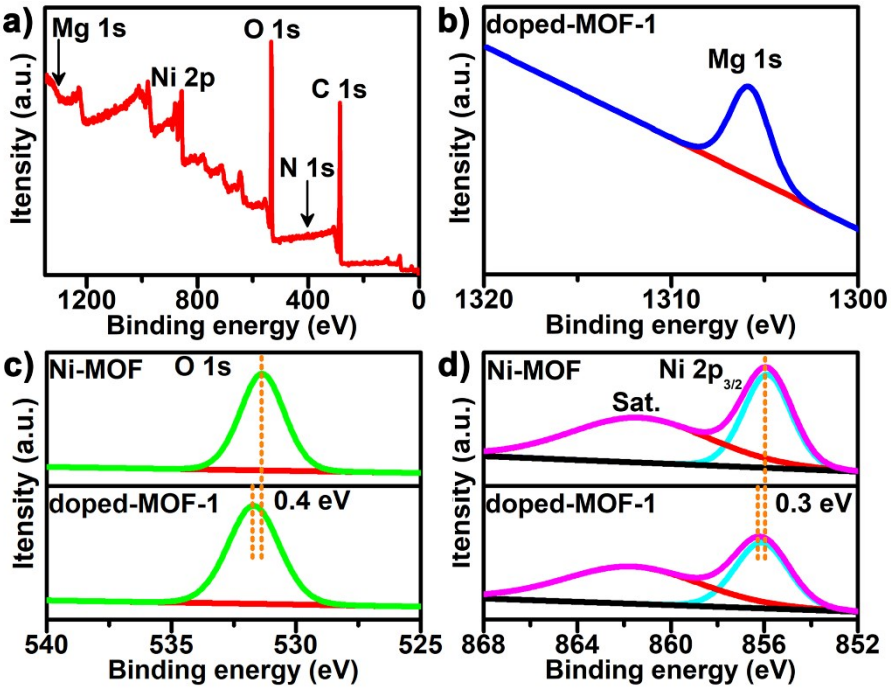

Fig. S8. XPS of survey spectra (a) and high-resolution Mg 1s spectra (b) of doped-MOF-1. Comparison of high-resolution O 1s (c) and Ni 2p (d) spectra between Ni-MOF and doped-MOF-1.

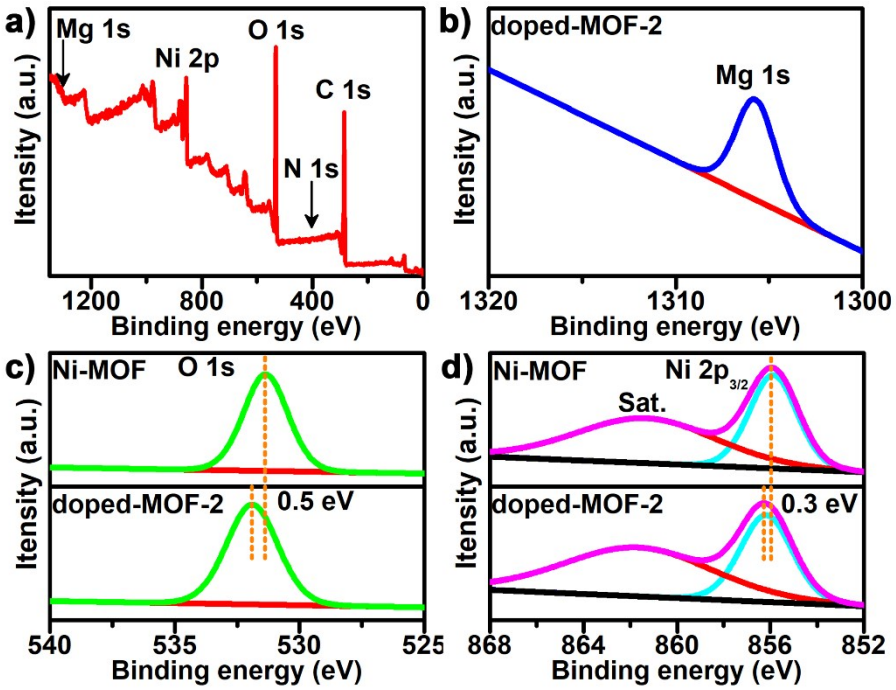

Fig. S9. XPS of survey spectra (a) and high-resolution Mg 1s spectra (b) of doped-MOF-2. Comparison of high-resolution O 1s (c) and Ni 2p (d) spectra between Ni-MOF and doped-MOF-2.

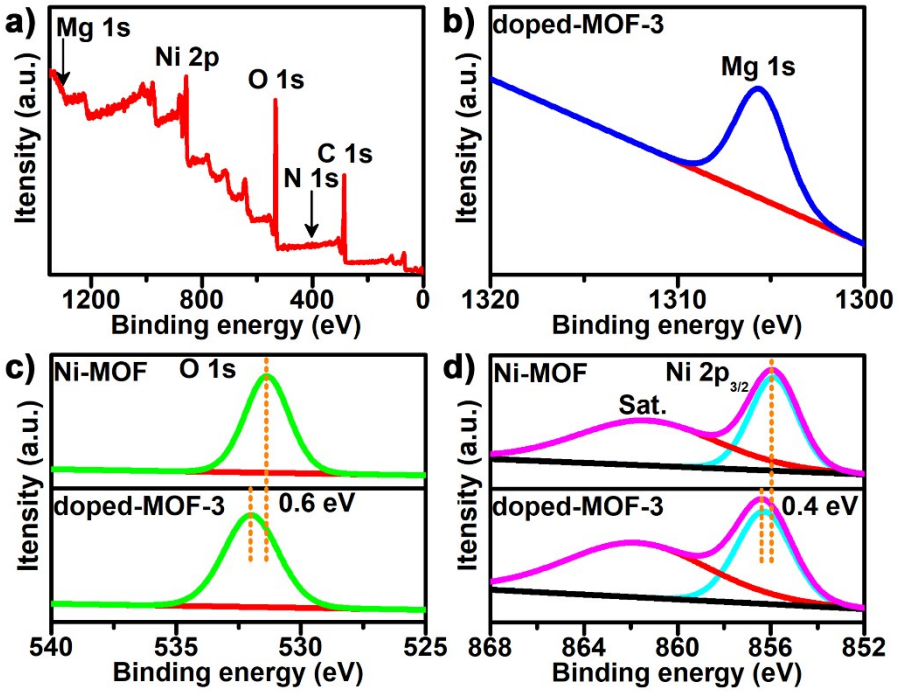

Fig. S10. XPS of survey spectra (a) and high-resolution Mg 1s spectra (b) of doped-MOF-3. Comparison of high-resolution O 1s (c) and Ni 2p (d) spectra between Ni-MOF and doped-MOF-3.

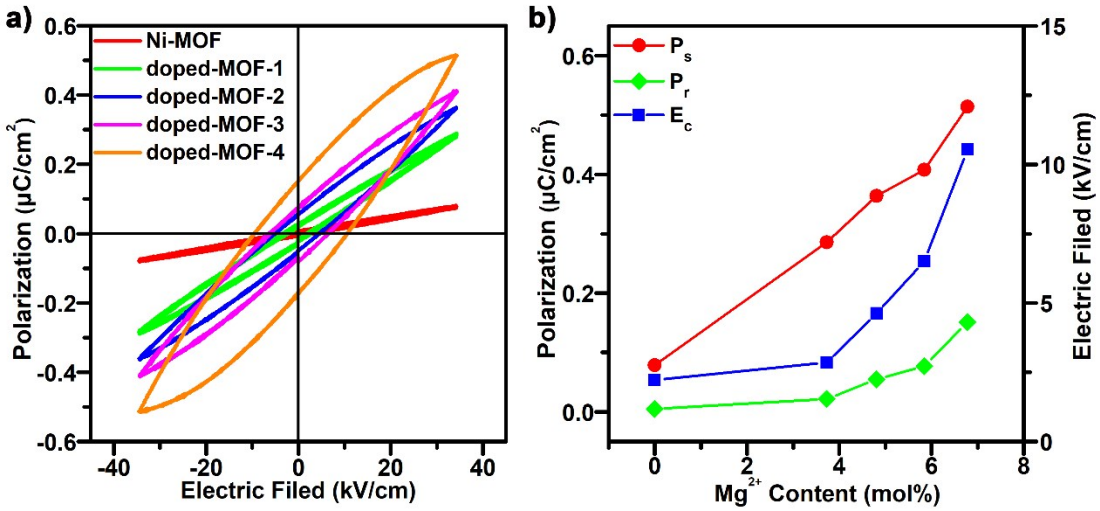

Fig. S11. Room-temperature polarization-electric field (P-E) characteristics (a) as well as Mg^{2+} concentration dependence of polarization and coercive field (b) of Ni-MOF and doped-MOFs at field of 27.6 kV/cm.

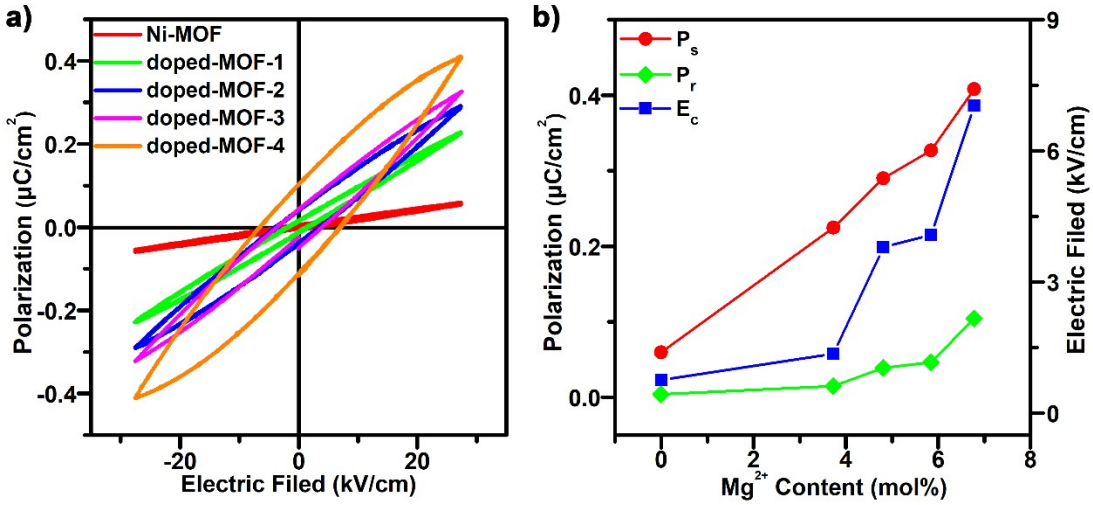

Fig. S12. Room-temperature polarization-electric field (P-E) characteristics (a) as well as Mg^{2+} concentration dependence of polarization and coercive field (b) of Ni-MOF and doped-MOFs at field of 34.5 kV/cm.

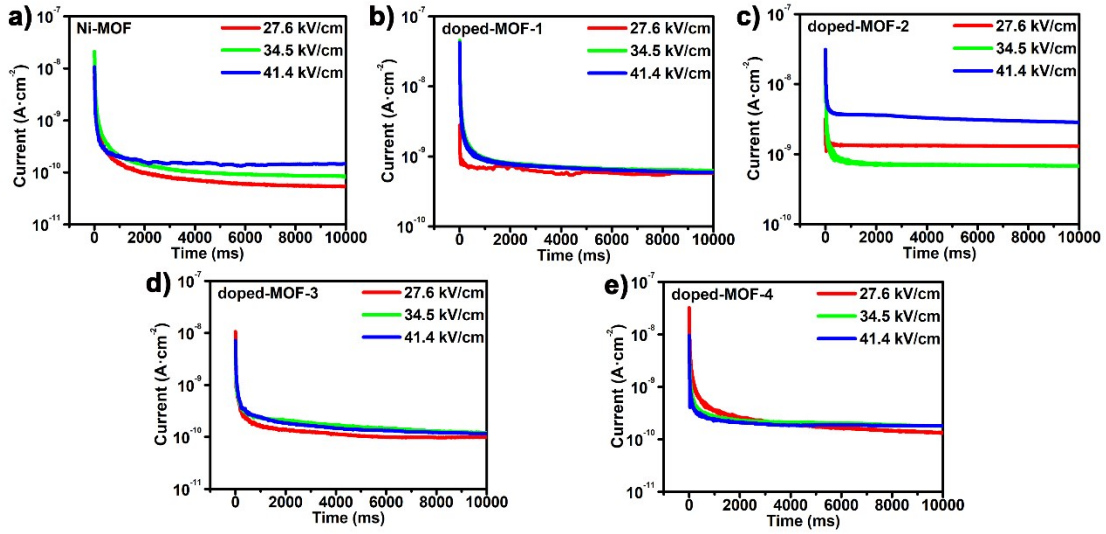

Fig. S13. Leakage current of Ni-MOF (a), doped-MOF-1 (b), doped-MOF-2 (c), doped-MOF-3 (d), and doped-MOF-4 (e) under various electric field at room temperature.

Reference:

1. C. Pan, J. Nan, X. Dong, X. M. Ren and W. Jin, *J. Am. Chem. Soc.*, 2011, **133**, 12330-12333.
2. L. Yu, X.-N. Hua, X.-J. Jiang, L. Qin, X.-Z. Yan, L.-H. Luo and L. Han, *Cryst. Growth Des.*, 2014, **15**, 687-694.
3. Y. Z. Tang, M. Zhou, J. Huang, Y. H. Tan, J. S. Wu and H. R. Wen, *Inorg. Chem.*, 2013, **52**, 1679-1681.
4. W. J. Ji, Q. G. Zhai, S. N. Li, Y. C. Jiang and M. C. Hu, *Chem. Comm.*, 2011, **47**, 3834-3836.
5. L. N. Zhang, S. Y. Guan, Y. C. Fan, C. X. Du, D. Zhao and B. Z. Liu, *Z. Krist. – Cryst. Mater.*, 2019, **234**, 33-41.
6. W. W. Zhou, J. T. Chen, G. Xu, M. S. Wang, J. P. Zou, X. F. Long, G. J. Wang, G. C. Guo and J. S. Huang, *Chem. Comm.*, 2008, **24**, 2762-2764.
7. A. K. Gupta, D. De, R. Katoch, A. Garg and P. K. Bharadwaj, *Inorg. Chem.*, 2017, **56**, 4698-4706.
8. Y.-T. Wang, G.-M. Tang, Y.-Q. Wei, T.-X. Qin, T.-D. Li, C. He, J.-B. Ling, X.-F. Long and S. Weng Ng, *Cryst. Growth Des.*, 2010, **10**, 25-28.